PNAS
www.pnas.org

Supplementary Information for

Cavitation controls droplet sizes in elastic media

Estefania Vidal-Henriquez and David Zwicker

Estefania Vidal-Henriquez.
E-mail: estefania.vidal@ds.mpg.de

This PDF file includes:

Supplementary text
Figs. S1 to S6
Captions for Movies S1 to S2
References for SI reference citations

Other supplementary materials for this manuscript include the following:

Movies S1 to S2

Supporting Information Text

1. Elastic energy of a growing cavity

We consider a droplet nucleated inside a cavity of an elastic material. This cavity has original radius A and we look for the elastic energy of the system once the droplet has grown and expanded the cavity to a radius a. The elastic energy F_E of the system is

$$F_E = \int \omega \mathrm{d}^3 r \ , \qquad [1]$$

where ω is the energy density of the system and depends on the elastic properties of the media. Assuming a spherical cavity and a perfectly homogenous system, the pressure P exerted on the droplet is

$$P = -\int \frac{2\sigma}{r} \mathrm{d}r \ , \qquad [2]$$

where σ is the biaxial stress and r the radial coordinate of the deformed solid. We parametrize the system using the radial stretch $\lambda = r/R$, where R is the radial coordinate in the original (non-deformed) solid. The two coordinates systems are related through volume conservation,

$$R^3 - A^3 = r^3 - a^3 \ . \qquad [3]$$

Using the biaxial stress definition

$$\sigma(\lambda) = \frac{\lambda}{2} \frac{\mathrm{d}\omega}{\mathrm{d}\lambda}, \qquad [4]$$

we obtain the pressure P in terms of the energy density,

$$P = \int_1^{a/A} \frac{1}{\lambda^3 - 1} \frac{\mathrm{d}\omega}{\mathrm{d}\lambda} \mathrm{d}\lambda \ , \qquad [5]$$

where we have used $\lambda \to 1$ at the system's boundary. Integrating by parts we obtain

$$P = \left. \frac{\omega}{\lambda^3 - 1} \right|_1^{a/A} + \int_1^{a/A} \frac{3\lambda^2 \omega}{(\lambda^3 - 1)^2} \mathrm{d}\lambda \ . \qquad [6]$$

Defining

$$P_0 = \frac{A^3 \omega(a/A)}{a^3 - A^3}, \qquad [7]$$

and using the definition of Elastic Energy F_E, we get an expression for the elastic energy in terms of the pressure exerted on the droplet

$$F_E = \frac{4\pi(a^3 - A^3)}{3}(P - P_0). \qquad [8]$$

We next check whether this mechanical definition is consistent with the thermodynamic definition

$$\frac{\partial F_E}{\partial V} = P, \qquad [9]$$

where F_E is differentiated with respect to the expanded cavity radius $V = 4\pi a^3/3$. Differentiating Eq. (8),

$$\frac{\partial F_E}{\partial V} = P - P_0 + \frac{(a^3 - A^3)}{3a^2} \left(\frac{\partial P}{\partial a} - \frac{\partial P_0}{\partial a} \right) \ , \qquad [10]$$

using the definition of P_0, see Eq. (7), we find

$$\frac{\partial F_E}{\partial V} = P + \frac{1}{3a^2} \left((a^3 - A^2) \frac{\partial P}{\partial a} - A^3 \frac{\partial \omega}{\partial a} \right) \ . \qquad [11]$$

Finally, using Eq. (5), we obtain

$$\frac{\partial P}{\partial a} = \frac{A^3}{a^3 - A^3} \frac{\partial \omega}{\partial a}, \qquad [12]$$

which combined with Eq. (11) recovers the thermodynamic pressure given by Eq. (9).

2. Free energy of a growing droplet

We now look for a simple expression for the free energy of a growing droplet in a phase separating system. Analysing how this energy changes with volume will give us an approximation of the effect of an external pressure in this system.

Given a free energy density f and a systems's size $V_{\rm sys}$, the total free energy is

$$F = Vf(\phi_{\rm in}) + (V_{\rm sys} - V)f(\phi_{\rm out}) + \gamma A + F_E(V) \ , \tag{13}$$

where $\phi_{\rm in}$ is the volume fraction inside the growing droplet, $\phi_{\rm out}$ is the volume fraction outside, F_E is, as before, the elastic energy, V is the droplet's volume, and A is the droplet's surface area.

We assume material conservation in the system during the droplet's expansion,

$$V_{\rm sys}\bar{\phi} = (V_{\rm sys} - V)\phi_{\rm out} + V\phi_{\rm in} \ , \tag{14}$$

where $\bar{\phi}$ is the average concentration in the system. Assuming small changes in the dilute phase concentration, we can expand the free energy density,

$$f(\phi_{\rm out}) \approx f(\phi^0_{\rm out}) + f'(\phi^0_{\rm out}) \left(\frac{V_{\rm sys}\bar{\phi} - V\phi_{\rm in}}{V_{\rm sys} - V} - \phi^0_{\rm out} \right) . \tag{15}$$

We can then reorder the free energy as

$$F \approx F_0 - Vg + \gamma A + F_E \ , \tag{16}$$

with

$$g = f(\phi^0_{\rm out}) - f(\phi_{\rm in}) + f'(\phi^0_{\rm out})(\phi_{\rm in} - \phi^0_{\rm out}) \tag{17}$$

and

$$F_0 = V_{\rm sys}\left[f(\phi^0_{\rm out}) + f'(\phi^0_{\rm out})(\bar{\phi} - \phi^0_{\rm out}) \right] \ . \tag{18}$$

Using the definition of osmotic pressure,

$$\Pi = -f(\phi) + f'(\phi)\phi \ , \tag{19}$$

we express g using the difference in osmotic pressures,

$$g = \Pi_{\rm in} - \Pi^0_{\rm out} - \left[f'(\phi_{\rm in}) - f'(\phi^0_{\rm out}) \right] \phi_{\rm in} \ . \tag{20}$$

Finally, using the definition of chemical potential $\mu = \nu f'(\phi)$, with ν the molecular volume, we obtain

$$g = \Pi_{\rm in} - \Pi^0_{\rm out} - \left[\mu_{\rm in} - \mu^0_{\rm out} \right] c_{\rm in} \ , \tag{21}$$

where $c_{\rm in} = \phi_{\rm in}/\nu$ is the number concentration inside the droplet. In the case of an incompressible dense phase, i.e. where $\phi_{\rm in}$ is constant, we find that the driving strength g is independent of droplet volume.

3. Stability analysis

We showed in the previous section that the driving strength g is typically independent of the droplet volume V. Phase separation is favorable (in the absence of surface tension and elastic effects), when $g > 0$. To see how elastic effects affect the phase separation, we differentiate Eq. (16) with respect to the droplet volume,

$$\frac{\partial F}{\partial V} = -g + \frac{2\gamma}{R} + P_E \ , \tag{22}$$

where we have used Eq. (9) to derive the elastic pressure. Therefore, droplet growth is favourable if

$$g > \frac{2\gamma}{R} + P_E \ . \tag{23}$$

A droplet will thus grow as long as the driving strength g is bigger than the total pressure difference between the inside and outside of the droplet.

We next study the stability of a steady state, which exists when $g = P(R^*)$. This state is stable if

$$\left.\frac{\partial^2 F}{\partial V^2}\right|_{R=R^*} = \left.\frac{\partial}{\partial V}\left(\frac{2\gamma}{R} + P_E(R)\right)\right|_{R=R^*} > 0 \ . \tag{24}$$

Therefore, a droplet will be stable if the pressure increases with increasing radius.

The same stability condition can be obtained from the dynamical equations presented in the main manuscript,

$$\frac{{\rm d}R_i}{{\rm d}t} = \frac{D}{R_i c_{\rm in}}\left[c(\vec{x}_i) - c_{\rm eq}\big(P(R_i), T\big) \right] \ . \tag{25}$$

A linear stability analysis shows that the droplet radius is stable if $c_{\rm eq}$ increases with droplet radius. Since $c_{\rm eq}$ is a monotonically increasing function of $P(R)$, the stability condition reduces to

$$\left.\frac{\partial}{\partial R}\left(\frac{2\gamma}{R} + P_E(R)\right)\right|_{R=R^*} > 0 \ , \tag{26}$$

which is equivalent to Eq. (24).

4. Droplet nucleation

We here study the droplet nucleation behavior by considering the energy necessary to cross the nucleation barrier in the absence of elastic effects. We consider a supersaturated homogeneous solution with concentration c_0 and use the driving strength g, Eq. (21), to estimate the energy change due to a droplet nucleating. We assume that the differences in pressure relax much more quickly than the differences in chemical potential, implying that we can approximate the driving strength as

$$g \approx [\mu_{\text{out}} - \mu_{\text{in}}]c_{\text{in}} \, . \tag{27}$$

To estimate its value, we thus need to determine the chemical potentials μ_{out} and μ_{in} outside and inside the droplet, respectively.

Assuming that the nucleated droplet is small, the chemical potential outside is close to that of the homogeneous phase, which can be estimated using ideal solution theory, $\mu_{\text{out}} \approx k_{\text{B}}T \log c_{\text{out}}$. To obtain an upper bound on the nucleation rate, we seek the strongest possible driving strength and thus use $c_{\text{out}} \approx c_0$.

We estimate the chemical potential μ_{in} inside the droplet by considering the phase separated system, which reached an equilibrium between a dilute phase with concentration $c_{\text{out}}^{\text{eq}}$ and a droplet phase with concentration $c_{\text{in}}^{\text{eq}}$. In equilibrium, the chemical potential of both phases are identical, and we thus have

$$\mu_{\text{in}}^{\text{eq}} = \mu_{\text{out}}^{\text{eq}} \approx k_{\text{B}}T \log(c_0 - \Delta c), \tag{28}$$

where $c_0 - \Delta c$ is a lower bound for the concentration in the dilute phase. Finally, we assume that the chemical potential inside the droplet is constant during equilibration, $\mu_{\text{in}} \approx \mu_{\text{in}}^{\text{eq}}$, to obtain the estimate

$$g \approx k_{\text{B}}T c_{\text{in}} \log\left(\frac{c_0}{c_0 - \Delta c}\right) . \tag{29}$$

Consequently, the change in free energy $\Delta\mathcal{F}$ due to one droplet of radius R is

$$\Delta\mathcal{F} \approx 4\pi R^2\gamma - \frac{4\pi}{3}R^3 g \, , \tag{30}$$

where $\gamma = 4.4\,\text{mN/m}$ is the surface tension measured in the experiments (1). The location of the maximum of this curve corresponds to the nucleation radius

$$R_{\text{nuc}} = \frac{2\gamma}{g} \approx 3.09\,\text{nm} \, , \tag{31}$$

where we have used the measured value $c_{\text{in}}k_{\text{B}}T = 11\,\text{MPa}$ (2). The associated energy barrier is

$$\Delta\mathcal{F}_{\text{nuc}} = \frac{16\pi\gamma^3}{3g^2} \approx 1.76 \cdot 10^{-19}\,\text{J} \approx 42.4\,k_{\text{B}}T \, . \tag{32}$$

The probability P_{nuc} of droplet nucleation can then be estimated using classical nucleation theory,

$$P_{\text{nuc}} = ke^{-\Delta\mathcal{F}_{\text{nuc}}/k_{\text{B}}T} \approx k \cdot 10^{-19} \, . \tag{33}$$

The pre-factor k in this theory is difficult to estimate, but this expression shows that the nucleation rate is suppressed by 10^{-19} and homogeneous nucleation is thus very unlikely in this system.

The fact that droplets appear in the experiments suggests that they are nucleated by alternative paths. We thus propose that heterogeneous nucleation is crucial. In heterogeneous nucleation droplets are nucleated around surfaces or imperfections, which effectively lower the nucleation barrier. The interaction of the droplet with these nucleation sites scales with the contact area, which scales with $\propto R^2$ if the size of the nucleation site is about R_{nuc} or larger. Consequently, the primary effect of heterogeneous nucleation is to lower the effective surface tension. We thus assume that our system for small droplets has an effective surface tension that is smaller than the measured surface tension for large cavitated droplets. We thus do not discuss surface tension effects in the main text and rather assume that droplet nucleation happens quickly.

5. Results are independent of mesh size and cavitation radius

In the Breakage model, we use a simplified pressure curve, which is parameterized by the mesh size ℓ, the cavitation radius R_{cav}, the cavitation pressure P_{cav}, the heterogeneity parameter η, and the final pressure P_∞ for large radii; see Fig. S1. The mesh size ℓ only determines when the pressure starts to increase, and therefore the slope of the pressure curve. Considering the cavitated droplet density n, introducing variation in the mesh size ℓ is equivalent to variations in P_{cav} for different droplets. Beside this, varying the mesh size ℓ changes the size of the small droplets, but since they do not affect the number of cavitated droplets, we do not study this effect further. We thus for simplicity only vary P_{cav} and keep ℓ the same for all droplets. Moreover, numerical simulations indicate that the cavitation radius R_{cav} has basically no influence on the cavitated droplet density n; see Fig. S2. Given these results we choose not to vary R_{cav} between droplets or simulations, and keep η/m as our only free parameter to fit experimental data.

6. Ostwald Ripening

In this section we estimate the relevant timescale for Ostwald ripening in our system to asses its relevance for the cavitated droplets. Ostwald ripening is driven by surface tension and the relevant scale is the capillary length scale ℓ_γ of the system (3),

$$\ell_\gamma = \frac{2\gamma}{c_{\rm in} k_{\rm B} T} \approx 0.8\,{\rm nm}\ , \tag{34}$$

where we have used the surface tension $\gamma = 4.4\,{\rm mN/m}$ of macroscopic droplets (1). Linear stability analysis shows that the fastest growing mode λ is given by (4)

$$\lambda = \frac{D\ell_\gamma}{R^3}\frac{c_{\rm eq}}{c_{\rm in}}\ . \tag{35}$$

Considering a typical radius $R = 10\,\mu{\rm m}$ of a cavitated droplet, together with $D = 50\,\mu{\rm m}^2/{\rm s}$ and $c_{\rm eq}/c_{\rm in} \approx c_{\rm sat}(300\,{\rm K})/c_{\rm in} = 0.054$, we find $\lambda \approx 2.14\cdot\ 10^{-6}\,{\rm s}^{-1}$. Consequently, the timescale $\tau = \lambda^{-1}$ of Ostwald ripening between the cavitated droplets is

$$\tau \approx 130\,{\rm hr}\ . \tag{36}$$

Interestingly, the same expression is obtained when considering the critical radius R_c of the Lifshitz–Slyozov scaling law (3)

$$R_c \propto \left(\frac{D\ell_\gamma c_{\rm eq}}{c_{\rm in}} t\right)^{1/3}\ . \tag{37}$$

We thus conclude that Ostwald ripening is a slow process in our system and we can neglect it.

7. Numerical Simulations with Nucleation

To make a more realistic comparison of the Neo-Hookean model and the Breakage model, we performed numerical simulations with a simple droplet nucleation protocol. The simulations were initialized without any droplets and at each time step a droplet might nucleate with a probability $p_{\rm nuc}$. The new droplet appears with $R < \ell$. The typical simulations presented in Figure S3 show that in the Neo-Hookean model the new droplets can grow freely, leading to a wide range of final radii. In contrast, in the Breakage model, most new droplets get stuck at mesh size and do not grow further, thus producing a monodispersed emulsion of cavitated droplets.

8. Pair correlation function

To quantify the position correlations of droplets in our system we defined the pair correlation function $g(r)$ which gives the probability of finding a droplet at distance r from the reference droplet. It is formally defined as

$$g(r) = \frac{V_{\rm sys}}{N}\left\langle \sum_i \delta(\vec{r} - \vec{r_i}) \right\rangle\ , \tag{38}$$

where the sum is over all cavitated droplets, the average is over different ensembles, N is the number of cavitated droplets, and $V_{\rm sys}$ the system's volume. In practice we calculate it as

$$g(r) = \frac{h(r) V_{\rm sys}}{4\pi N^2 r^2 \Delta r}\ , \tag{39}$$

where $h(r)$ is the histogram of the distances between droplets (a total of $N(N-1)$ elements) and Δr is the histogram's bin size. Finally, to collapse the different curves we normalized by the mean droplet distance $2[3/(4\pi n)]^{1/3}$.

9. Theoretical estimation of cavitated droplet density n

We here provide details on the analytical theory to predict the density n of cavitated droplets. This is based on the simplified picture that a single large droplet depletes a surrounding volume of radius L in a diffusion limited process. To obtain the concentration field around this droplet, we solve Eq. (6) in a spherical domain of radius $L = [3/(4\pi n)]^{1/3}$ with boundary conditions $\partial_r c|_{r=L} = 0$ and $c(r = R_{\rm cav}) = c_{\rm sat}(t)\exp\left(P_\infty/(c_{\rm in} k_B T)\right)$. Defining $\bar{c} = c + \alpha t \exp\left(P_\infty/(c_{\rm in} k_B T)\right)$ turns Eq. (6) into

$$\partial_t \bar{c} = D\nabla^2 \bar{c} + \alpha \exp\left(\frac{P_\infty}{c_{\rm in} k_B T}\right) - c_{\rm in}\sum_i \frac{{\rm d}V_i}{{\rm d}t}\delta(\vec{x_i} - \vec{x})\ , \tag{40}$$

with the simpler boundary conditions $\partial_r \bar{c}|_{r=L} = 0$ and $\bar{c}(r = R_{\rm cav}) = c_0 \exp\left(P_\infty/(c_{\rm in} k_B T)\right)$. Assuming radial symmetry and steady state, the field around a cavitated droplet of radius $R_{\rm cav}$ reads

$$\begin{aligned}\bar{c}(r) = \Bigg[c_0 + \frac{\alpha}{6D}\left(R_{\rm cav}^2 - r^2\right) \\ + \frac{\alpha L^3}{3D}\left(\frac{1}{R_{\rm cav}} - \frac{1}{r}\right)\Bigg] \exp\left(\frac{P_\infty}{c_{\rm in} k_B T}\right)\ .\end{aligned} \tag{41}$$

We thus simplified the cavitation scenario by assuming that once a droplet cavitates it absorbs material in a sphere of radius L around them.

To account for heterogeneity in the cavitation pressures $P_{\rm cav}$, we describe them through their cumulative distribution function $F(P_{\rm cav})$, which gives the fraction of droplets whose cavitation pressure is lower than $P_{\rm cav}$. Since only droplets with the lowest cavitation thresholds will cavitate, we only need to describe the lower end of $F(P_{\rm cav})$. Since there must be a lowest, positive cavitation pressure $P_{\rm cav}^{\rm min}$, we assume a linear expansion around this minimum,

$$\mathcal{F}(P_{\rm cav}) = \frac{P_{\rm cav} - P_{\rm cav}^{\rm min}}{\eta}\Theta(P_{\rm cav} - P_{\rm cav}^{\rm min}) \,, \tag{42}$$

where η describes how widely distributed the lower thresholds are. This expression can be rewritten using Eq.(5) to obtain the cumulative distribution in terms of the equilibrium concentrations.

$$\begin{aligned}\mathcal{F}(c,t) = &\left[\frac{c_{\rm in}k_BT}{\eta}\log\left(\frac{c}{c_0-\alpha t}\right) - \frac{P_{\rm cav}^{\rm min}}{\eta}\right] \\ &\Theta\left(c_{\rm in}k_BT\log\left(\frac{c}{c_0-\alpha t}\right) - P_{\rm cav}^{\rm min}\right) \,.\end{aligned} \tag{43}$$

Therefore, given a density m of nucleated droplets, the density of droplets with cavitation threshold below c is $m\mathcal{F}(c,t)$. For this theory to be self-consistent, the aforementioned volume $V = n^{-1}$ must have only one droplet with a cavitation threshold below the concentration field, i.e.

$$1 = 4\pi\int_0^L m\mathcal{F}(c(r),\bar{t})r^2dr. \tag{44}$$

Here, we take the time $\bar{t}$ such that the equilibrium concentration of the n-th droplet matches the total amount of material in the system c_0,

$$\bar{t} = \frac{c_0}{\alpha}\left[1 - \exp\left(\frac{-P_{\rm cav}^{\rm min} - \eta n/m}{c_{\rm in}k_BT}\right)\right] \,. \tag{45}$$

We can now combine Eq. (41)-(45) to obtain an implicit relation for the cavitated droplet density n, which we solve numerically to obtain the lines shown in the main text.

10. Temperature protocol changes

Numerical simulations, where the cooling rate is increased after droplet cavitation, show that a new group of droplets can cavitate if the new rate is high enough. Examples of this type of simulations are shown in Fig. S5 and Fig. S6. We show in Eq. (41) that the concentration profile around a cavitated droplet depends strongly on the material rate α. If this rate is suddenly increased, the new concentration profile might be higher than the cavitation concentration $c_{\rm cav}$ of some of the small droplets, thus causing their cavitation. This process can then be repeated to cavitate additional droplets, as depicted in Fig. S6. Therefore, controlling the rate α allows to control the droplet size distribution.

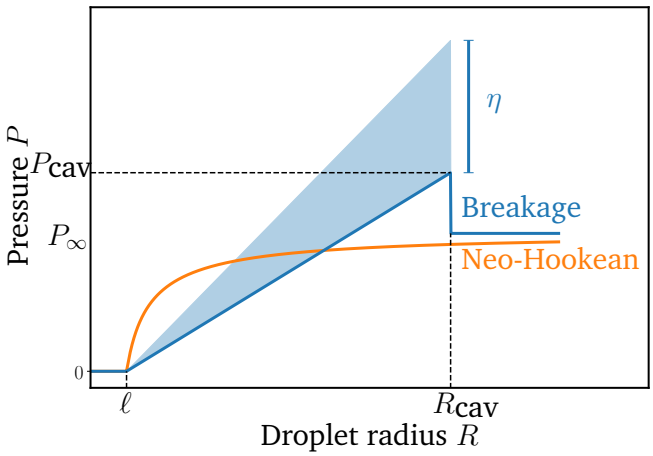

Fig. S1. Stress-strain relation of the Neo-Hookean and Breakage model. Pressure P as a function of the droplet radius R, which is imposed in numerical simulations. Breakage model in blue and Neo-Hookean model in orange. The plot indicates the mesh size ℓ, the radius R_{cav} at which the droplet cavitates, the maximal pressure P_{cav} the mesh can exert, and the pressure P_∞ after breakage. The shaded area shows the possible values for P_{cav} given the distribution parameter η.

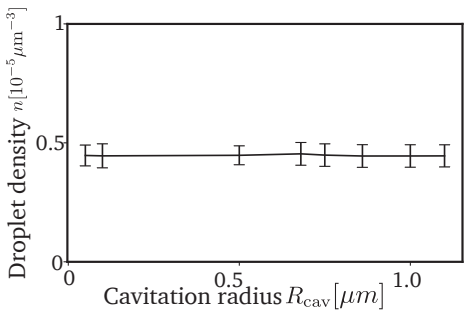

Fig. S2. Droplet density is independent of cavitation radius Density n of cavitated droplets as a function of the cavitation radius R_{cav}. Model parameters as in Fig. 2 of the main manuscript, except η/m = 3·10^5 E µm^3.

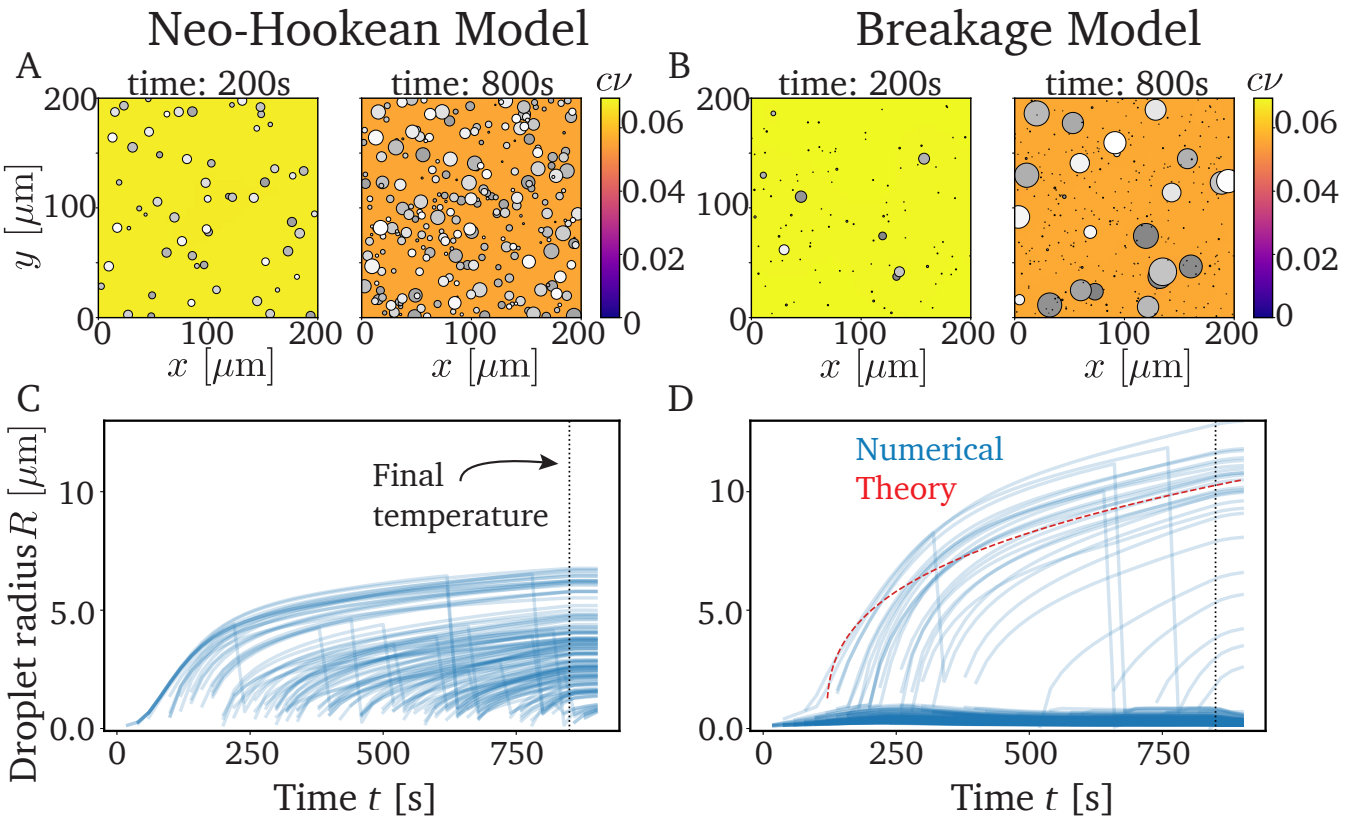

Fig. S3. Breakage stops newly nucleated droplets from growing. (A,B) Snapshots of a typical simulation with a constant nucleation rate for Neo-Hookean (left) and Breakage pressure curves (right). Disks indicate droplets, while the heat map indicates the concentration c in the dilute phase, gray scale indicates depth in the z-axis. (C,D) Droplet radii over time for all nucleated droplets. $p_{\mathrm{nuc}} = 0.5\,\mathrm{s}^{-1}$, other parameters as in Figure 2 of the main text.

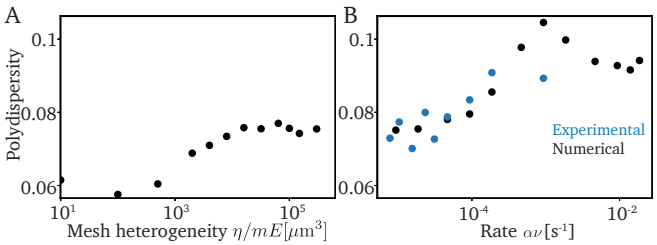

Fig. S4. Polydispersity increases at higher droplet densities. Polydispersity, defined as the standard deviation of the droplet radius divded by its mean, for (A) different mesh heterogeneities η/mE and (B) different rates α. Experimental data from (1).

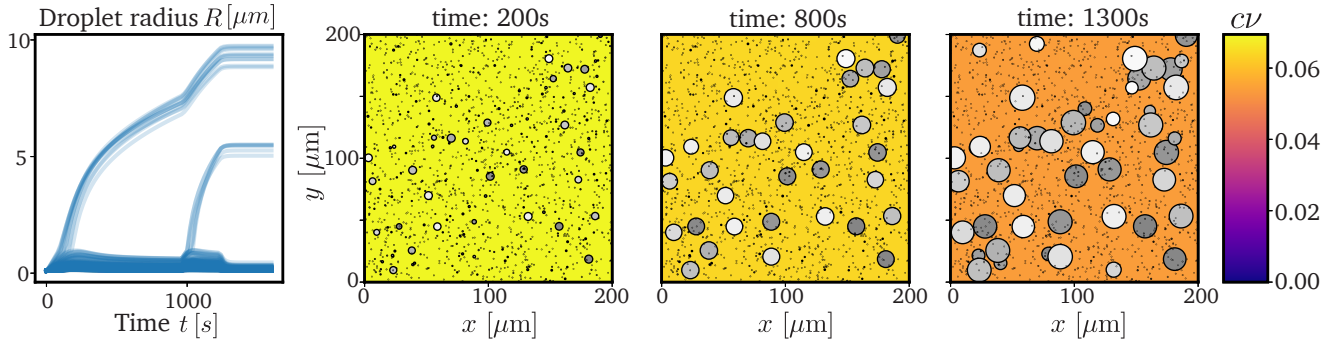

Fig. S5. Double quench experiment produces a bimodal distribution. Left panel: Droplet radii as a function of time displaying a bimodal distribution of the cavitated droplets and several small ones kept at mesh size. Subsequent panels: 2-D projection of a typical time evolution in this system, showing droplets starting to cavitate, grown first group of cavitated droplets, and final state of the system. Smaller droplets are shown as black dots for didactic purposes and might appear as inside cavitated droplets due to 3-D projection. Parameters are $\eta/m = 3{\cdot}10^5 E$ µm ^{3}, $E = 80$ kPa, first cooling rate $\alpha = 7.77{\cdot}10^{-6}$ s$^{-1}\nu^{-1}$, second cooling rate $\alpha = 3.11{\cdot}10^{-5}$ s$^{-1}\nu^{-1}$. Other parameters as in Figure 2.

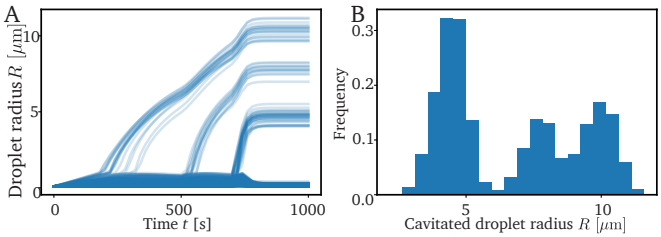

Fig. S6. Increasing rate stepwise leads to increasingly more droplet cavitating. Simulation increasing the material rate α twice during the cooling process. A) Droplet radii as a function of time displaying a trimodal distribution of the cavitated droplets and several small ones kept at mesh size. B) Radii probability distribution. Parameters are $\eta/m = 3{\cdot}10^5 E$ µm ^{3}, first cooling rate $\alpha = \alpha_0 = 7.77{\cdot}10^{-6}$ s$^{-1}\nu^{-1}$, second cooling rate $\alpha = 4\alpha_0$, and third cooling rate $\alpha = 16\alpha_0$. Other parameters as in Figure 2.

Movie S1. A typical numerical simulation showing cavitated droplet coexisting with small droplets. Same simulation as Figure 2.

Movie S2. Double Quench Simulation. Increasing the temperature change rate mid simulation produces a bimodal distribution of cavitated droplet radii. Same simulation as Figure S5.

References

1. Style RW, et al. (2018) Liquid-liquid phase separation in an elastic network. *Physical Review X* 8(1):011028.
2. Rosowski KA, et al. (2020) Elastic ripening and inhibition of liquid–liquid phase separation. *Nature Physics* 16(4):422–425.
3. Weber CA, Zwicker D, Jülicher F, Lee CF (2019) Physics of active emulsions. *Reports on Progress in Physics* 82(6):064601.
4. Zwicker D, Hyman AA, Jülicher F (2015) Suppression of Ostwald ripening in Active Emulsions. *Phys. Rev. E* 92:012317.